# Lowering the Water Oxidation Overpotential by Spin-Crossover in Cobalt Hexacyanoferrate

Franziska Simone Hegner,[*,†,‡] José Ramón Galán-Mascarós,[†,¶] and Núria López[†]

†*Institute of Chemical Research of Catalonia (ICIQ), The Barcelona Institute of Science and Technology (BIST), Avinguda Països Catalans 16, 43007 Tarragona, Spain.*

‡*Technical University of Munich (TUM), 85748 Garching, Germany.*

¶*ICREA, Passeig Lluís Companys 23, 08010 Barcelona, Spain.*

E-mail: fshegner@gmail.com

**Abstract**

The oxygen evolution reaction (OER) is limited by the inherent linear scaling relationships of its reaction intermediates. Manipulating the spin configuration of the water oxidation intermediates allows us to overcome these constraints. Cobalt hexacyanoferrate (CoFe–PB) is an efficient and robust water oxidation catalyst and further known as a magnetic switch. Its versatile electronic structure renders it a potential candidate for magnetic tuning of the OER. Here, we used high level density functional theory calculations to describe the OER on two different CoFe–PB model systems, and evaluated the possibility for spin-crossover (SCO) of its resting states. We show that SCO during OER can significantly lower the overpotential by 0.7 V, leading to an overpotential of around 0.3 V, which is in agreement with to the experimentally measured one. Applying an external potential >1.5 V vs. SHE the SCO-assisted pathway becomes largely favoured and most likely the predominant reaction pathway.

# Graphical TOC Entry

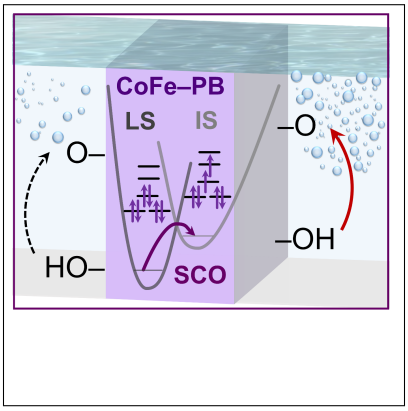


# Keywords

Cobalt hexacyanoferrate, Prussian blue analogues, water oxidation, oxygen evolution reaction, spin-crossover, minimum energy crossing points, scaling relationships

Green hydrogen, produced by solar or wind powered electrolysis of water, is one of the most promising clean energy carriers, storing intermittent renewables. Further, it serves as an important feedstock for the chemical industry, where it is still mainly produced from reforming natural gas or the gasification of coal.[1] Water electrolysis splits $H_2O$ into gaseous $H_2$ and $O_2$ via the Hydrogen Evolution Reaction (HER) at the electrolyzer cathode and the Oxygen Evolution Reaction (OER) at the anode, respectivley. Out of those, the OER is often considered to be the bottleneck to large scale industrial implementation. It can be divided into four concerted proton-coupled electron transfer (PCET) steps, considering the most common Water Nucleaophilic Attack (WNA) mechanism.[2,3]

$$\begin{aligned}
{}^*M - \square \; + \; H_2O \; &\rightleftharpoons \; {}^*M - OH \; + \; H^+ \; + \; e^- && (OER\,1) \\
{}^*M - OH \; &\rightleftharpoons \; {}^*M - O \; + \; H^+ \; + \; e^- && (OER\,2) \\
{}^*M - O \; + \; H_2O \; &\rightleftharpoons \; {}^*M - OOH \; + \; H^+ \; + \; e^- && (OER\,3) \\
{}^*M - OOH \; &\rightleftharpoons \; {}^*M - \square \; + \; O_2 \; + \; H^+ \; + \; e^- && (OER\,4)
\end{aligned} \tag{1}$$

Where ${}^*M$ denotes the active site, at which the reaction occurs, and $\square$ a vacancy. In the ideal case, each of those PCET steps would occur at an applied voltage $U_{appl}$ of 1.23 $V_{SHE}$, i.e., its thermodynamic redox potential under Standard Hydrogen Electrode (SHE) conditions, and no additional potential would be required to drive the overall reaction. In reality though, an extra potential, the overpotential $\eta = U_{appl}\,(\text{vs SHE}) - 1.23V$, is needed, which is due to the fact that some steps, usually $OER\,2$ and $OER\,3$, only occur at significantly higher voltages. Much current research effort is focussed on finding suitable water oxidation catalysts that lower the overpotential, are stable and made out of Earth-abundant materials, such as nickel, iron, or cobalt layered (oxy)hydroxides, oxide perovskites like $Br_{0.5}Sr_{0.5}Co_{0.8}Fe_{0.3}O_{3-x}$, and (inverse) transition metal oxide spinels.[4–6] It seems, however, that there is a limit to the minimum achievable overpotential, which apparently cannot be lowered to much less than 0.25–0.30 V. This was explained by the linear scaling of OOH and OH binding energies that restrain the maximum OER activity.[2,5,7,8]

One possibilty to overcome these limits and to break these linear scaling relationships, is tuning the magnetic configuration of the catalyst. While the effect of the electron spin has long been neglected in heterogeneous (electro)catalysis, it recently gained a lot of attention, as current reviews show.[3,9–11] Magnetic control was exerted, for instance, by applying an external magnetic field,[12,13] using ferromagnets[14–16] or chiral surfaces,[17–19] or by modulating the vacancy content.[20] The magnetic enhancement typically involves a collective effect of surface magnetic sites,.[11] where two spin-aligned OH radicals couple to preferentially form the biradicalic $O_2$ product.[18] These mechanisms, however, rely on a concerted interection between two metal-hydroxo entities, as in the I2M mechanism that is different to Equation 1.

Local effects, solely depending on the spin state of the catalytically active site, are less understood but play an important role in the most common, single-site WNA mechanism (Equation 1). The influence of unpaired electrons on the catalytic site was proven to be crucial by Shao-Horn's group,[21,22] where they show that magnetic states, i.e., singly occupied $d$ ($e_g$) orbitals, on the transition metal catalyst surface improve the intrinsic OER activity. Therefore, the ability to change the spin state of the active site gives us another handle to tune electrocatalysis by magnetic effects, and therefore another way to overcome the limits imposed by linear scaling. The interchange of spin on one atom, which is known as spin-crossover (SCO), can be induced by modulating the local environment, which in turn can be done by different external factors, like temperature and pressure.[23–27] Indeed, SCO was indeed recently described to determine oxygen evolution and reduction reactions in single atom doped carbon materials.[28,29] To the best of our knowledge SCO on a solid surface that directly enhances the OER activity has not been reported.

Prussian blue-type materials are known to easily undergo charge-transfer and SCO.[25,26,30] In particular, the cobalt–iron Prussian blue analogue cobalt hexacyanoferrate (CoFe–PB, Figure 1) has long been known to be a switchable molecular magnet.[24] The spin state of its Co constituent atoms can easily be tuned by external stimuli, such as temperature,[30,31] light,[24–26]

pressure,[32] electric[33] and other fields,[33] that change its local electronic environment and surrounding crystal field. Furthermore, CoFe–PB was found to be a highly robust, easy-to-prepare, and efficient OER catalyst, which can operate in a wide range of pH ($1 <$ pH $< 13$) and is made out of Earth-abundnt transition metals.[34–37] Given the versatility of its electronic structure, the idea that CoFe–PB may undergo SCO during OER is not far to seek.

In this work, we performed Density Functional Theory (DFT) to describe water oxidation on CoFe–PB. We investigated different charge and spin states of the CoFe–PB catalyst and calculated the thermodynamic overpotentials for all spin-allowed OER steps and combinations of such. We found that changing the spin configuration of the OH intermediate from low to intermediate spin lowers the overpotential, which can be rationalized by the favorable filling of $e_g$ orbitals or its half-metallicity, respectively. This thermodynamically less favorable spin state can be reached by spin-crossover at thermal energies, which lowers the overpotential significantly and gives rise to a favourable SCO-assisted OER pathway.

## Results and discussion

We considered two different models of the catalytic CoFe–PB surface, a periodic slab $Na_6Co(II)_6[Fe(III)(CN)_6]_6 \cdot {}_3H_2O$ and a bimetallic cluster $[Co(HNC)_4(H_2O)(NC)Fe(CN)_5]^{(-)}$ which are described in more detail in the SI and can be found on the ioChem-BD database[38] under the DOI 10.19061/iochem-bd-1-229.[39] Two initial oxidation states were assumed for the cluster, i.e., reduced Co(II)Fe(III) ($[Co(HNC)_4(H_2O)(NC)Fe(CN)_5]^-$, **cluster (R)**) and oxidized Co(III)Fe(III) ($[Co(HNC)_4(H_2O)(NC)Fe(CN)_5]$, **cluster (O)**), in order to investigate the influence of the initial charge state on the reaction mechanism. While the finite-size cluster model is beneficial for our purpose as it allows for direct tuning of the charges and multiplicities of its constitutents and also requires less computational effort, it loses some information such as on long-range effects. This is why we tested both the periodic surface

and the cluster and, as we will see later, they lead to qualitatively similar results.

In the system the Fe centres always remain octahedrally coordinated by cyanide ligands due to the strong Fe–C metal–ligand bonds of the $[Fe(CN)_6]$ units. It is one of the most robust metal complexes[40] and unlikely to dissociate neither during electrochemical water oxidation nor during synthesis. Therefore, only the Co centres can be catalytically active and its spin and charge state will be our focus: $d^6$ Co(III) can adopt low spin (LS), intermediate spin (IS), and high spin (HS) configurations, and $d^7$ Co(II) can adopt LS and HS states, as shown in Figure SX. We note that the surface Co centres have a reduced $C_{4v}$ symmetry, in contrast to the octahedrally coordinated bulk metals, but we keep the notations and $t_{2g}/e_g$ symmetry labels derived from $O_h$ fields for the sake of convenience.

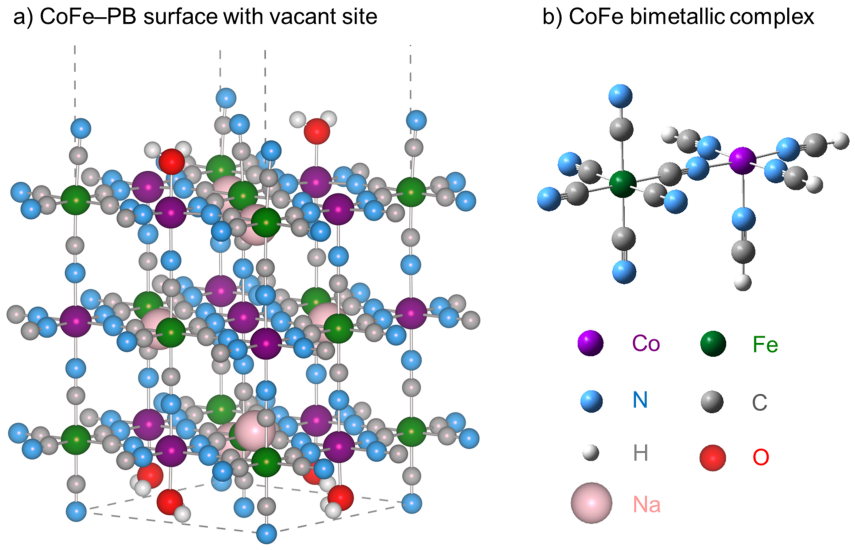


Figure 1: Cobalt hexacyanoferrate (CoFe–PB) model systems: a) a three-layered surface slab $Na_6Co_6[Fe(CN)_6]_6 \cdot 3\,H_2O$, calculated with the PBEsol+U ($U_{Co}$ = 3 eV, $U_{Fe}$ = 5 eV) functional. Fe centres are fully coordinated with $CN^-$ ligands and surface Co centres are coordinated by $H_2O$ (except active site), $Na^+$ ions are introduced to counterbalance the negative charge; b) a finite-size bimetallic Co–Fe cluster $[Co(HNC)_4(H_2O)(NC)Fe(CN)_5]^{(-)}$, calculated with the hybrid functional TPSSh; $NC^-$ ligands coordinated to Co are capped by H and all outer ligand atoms are fixed to present the embedding in the three-dimensional solid.

For modelling the OER mechanism we considered the single-site Water Nucleophilic Attack (WNA) mechanism, as in Equation 1 and shown in Figure 2. Catalytically active Co

centres are about 10 Å apart, which makes any concerted mechanism unlikely. We divide the reaction into four proton-coupled electron transfer (PCET) steps, which is advantageous as it allows us to calculate the reaction free energies of each step via Nørskov's Computational Hydrogen Electrode (CHE) formalism.[2,41] Thus we can set the chemical potential of an proton and an electron equal to that of $\frac{1}{2}$ $H_2$ and calculate the reaction free energies under SHE conditions (see SI for further details).

First, we calculated the energies and the properties of the different spin configurations of all intermediates, as well as the water coordinated surface *Co–$H_2O$, for all model systems (surface, cluster (R), and cluster (O)), which are listed in Tables S1 and S2, respectively. The most stable spin configuration is nearly always the overall low spin state with both LS Co and LS Fe (apart from the *Co–$H_2O$ and *Co–O structures on the solid surface). For Fe, which always resides in an LS state, this is expected due to their strong ligand field exerted by the C-site of the cyanide ligand.[40] Co, on the other hand, is coordinated from the cyanide's N-site, which is a medium field ligand and spin-pairing and ligand field splitting energies are of a similar magnitude. Small changes in the coordination sphere can lead to a switch between HS, IS, and LS configurations (for $d^6$ Co(III)), or between HS and LS (for $d^7$ Co(II)), respectively, see Figure SX. This explains i) why some Co centres, i.e., *Co(II)–$H_2O$ and *Co(III)–O on the solid surface, as well as fully –NC coordinated bulk Co(II) centres (not shown), prefer higher spin states, as they experience a slightly weaker ligand field, and ii) why Co in the bimetallic cluster always adopts an LS state because its capped -NCH ligands exert a stronger field than iron-bound -NC–Fe in the solid (a more detailed explanation can be found in the SI). We further note that consistent with previous calculations on Co complexes,[42] the *Co–O intermediate is always radicalic with unpaired electron density at the O site in all different Co spin configurations.

We now turn to the OER WNA mechanism as in Figure 2a. The reaction (free) energies for different pathways, including different spin configurations of the intermediates, are listed in Table S3. All those considered reaction pathways are spin-conserving,[43] whereas orbital

electronic conservation rules are relaxed due to vibrational-electronic coupling.[44] Spin-orbit coupling would form an exception but its effects are expected to be negligible.[45] Since in each PCET step we transfer one electron with a spin of $\pm\frac{1}{2}$, the overall spin of the system (CoFe–PB + adsorbate) is either reduced or increased by $\frac{1}{2}$.

Comparing the reaction energies for all systems, they all follow the same trend and, both cluster (R) and (O) show no significant differences. This indicates that (i) the simplified finite-size cluster is a valid model system to describe the OER on the CoFe–PB surface and (ii) the initial charge state does not play a role for the reaction energies. The former is very important, as it allows us to use the cluster for our considerations, which drastically reduces computational costs (by orders of magnitude, c.f. surface slab) and gives us control over charge and magnetisation of all atoms in the system, which aids the convergence of different magnetic solutions. Henceforth, we will here focus on the description of cluster (R), while the other systems and further discussion is given in the SI.

When considering the reaction path of only the lowest energy intermediates, that is the overall LS state, the second step ($OER\,2$), which corresponds to the abstraction of a proton and an electron from *Co–OH to form *Co–O, is most energetically demanding (see Table S3 and Figure SX). It therefore requires the largest potential and is termed potential determining step (PDS), with an energy of $\Delta G = 1.96$ eV ($\eta = 0.73$ V). This relatively high energy cost is due to the fact that LS Co(III) as in the *Co–OH intermediate has no unpaired electrons ($t_{2g}^6 e_g^0$ configuration), as shown in its (absent) spin density in Figure 2b (on the right). Thus the electron density is more localized at the Co centre, not contributing to the intermediate binding and not allowing for a facile electron transfer from the hydroxy OH group to the radicalic *Co–O.[46]

If, however, we include other spin configurations, not only the most stable LS state, other possible OER pathways can occur as described in the SI (Figures SX). Taking the IS configuration that is the second highest in energy (second pathway in Table S3 and Figure SX), the second step ($OER\,2$) from IS *Co–OH to IS *Co–O becomes less energetically

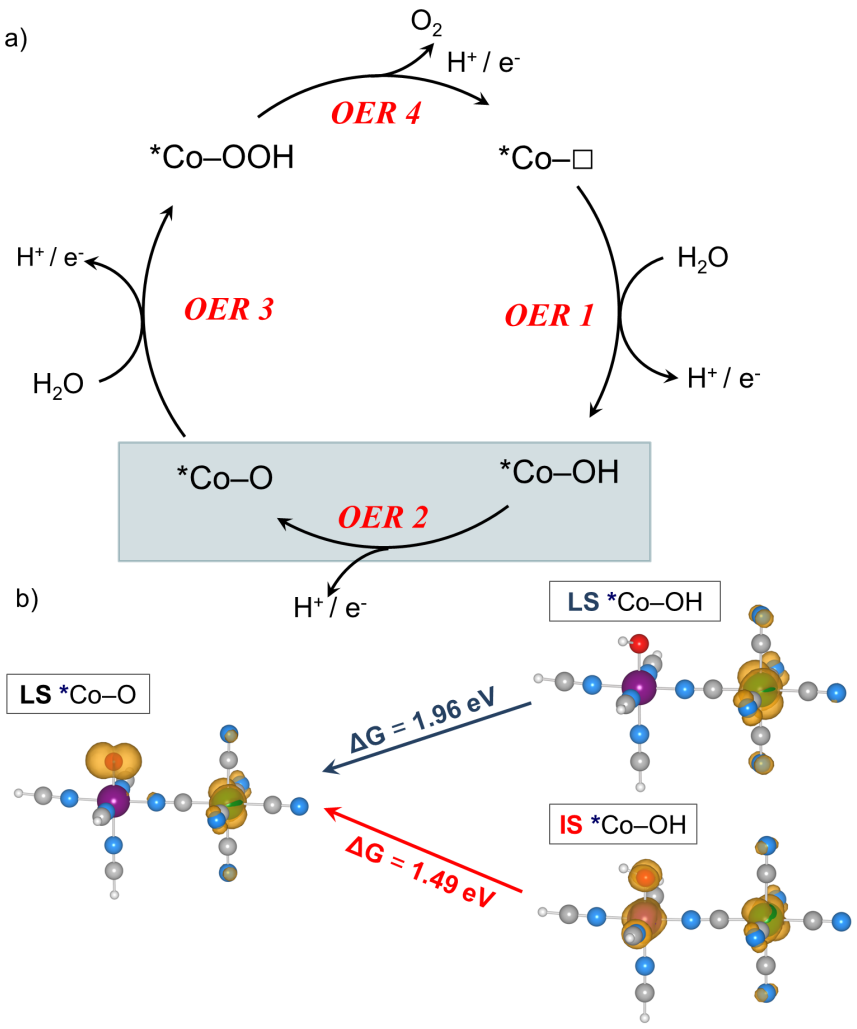


Figure 2: a) Catalytic OER cycle of the Water Nucleophilic Attack (WNA) mechanism, which is divided into four proton-coupled electron transfer (PCET) steps ($OER\ 1-4$), where *Co denotes the active site and □ a vacancy. In the pathway accounting for lowest intermediate configurations, $OER\ 2$ is the Potential Determining Step (PDS), in the grey box. b) Reaction free energies and spin densities involved in $OER\ 2$, i.e., the transition from *Co–OH to *Co–O, for both LS *Co–OH and IS *Co–O. The electronic spin densities with the yellow isosurface (0.005) present the charge density difference between majority and minority spin. For LS *Co–OH there is no spin density on the active Co site, whereas for IS *Co–OH there is, facilitating electron transfer. It is noted that in all intermediates the spin density on LS Fe(III) stays constant.

demanding and requires an overpotential $\eta = 0.31$ V ($\Delta G = 1.54$ eV). This transition becomes even lower for IS *Co–OH to LS *Co–O (third pathway in Table S3 and Figure SX), which is also spin-allowed, with an overpotential $\eta = 0.26$ V ($\Delta G = 1.49$ eV). These overpotentials agree better with the experimentally observed one of around 0.3 eV.[34,36,37] This also is in line with previous findings, in which Co in a higher spin state lowered the PCET transition energies.[13,14,16,46,47] The reason for lowering the energy barrier of $OER\,2$ is that IS *Co–OH possesses unpaired electrons in its $e_g$ orbital, as well as to a small extent localized on the hydroxy OH, which can be seen in its spin density in Figure 2b. This allows for a more efficient, spin-selective electron transfer and proton abstraction from IS *Co–OH. A similar phenomenom was already shown by Shao-Horn's group,[21,22] where they demonstrated that an $e_g$ occupation close to unity is favourable. In the language of solids, we can describe it as a half-metal with an overall ferromagnetic exchange delocalization (see Figure SX), which has also been found to enhance OER activity.[14,15] In those mechanisms with IS *Co–OH as active species (pathways 2 and 3 in Table SX and Figure SX), the first step ($OER\,1$) becomes the PDS with $\Delta G = 1.84$ eV ($\eta = 0.61$ V) in those mechanisms. Considering purely electrochemical steps, this formation of the IS *Co–OH intermediate ($OER\,1$) is extremely unlikely and as first step solely LS *Co–OH will be formed, which is the resting state in the LS pathway (Figure SX).

Nonetheless, we do not only need to allow for electrochemical steps: We know that Prussian blue-type materials, and in particular CoFe–PB,[24] can easily undergo charge-transfer and spin-crossover (SCO) under various conditions.[25,26,30,32] So, we wondered what if the LS *Co–OH resting state transitions to IS *Co–OH via SCO as schematized in Figure 3. To evaluate this possibility, we computed the minimum energy crossing points (MECP) between the potential energy surfaces (PES) of the two different magnetic states with the MECP program developed by Harvey et al.,[48,49] which is described in the SI. Table SX shows the energies and properties of the MECPs for the *Co–OH intermediates of clusters (R) and (O), as well as of the *Co–O and *Co–OOH intermediates (the latter are not relevant for the main discussion

but are described in the SI). We found that the energy barrier ($\Delta G_{SCO}$), i.e. the free energy needed to reach the MECP from LS *Co–OH is about 0.45 eV. The energy of the MECP energy is very close to the final IS *Co–OH state and, following Hammond's postulate,[50] so is the geometry of the MECP, e.g., the Co–O bond distance. Therefore, reaching IS *Co–OH through SCO may be slow but accessible at room temperature.

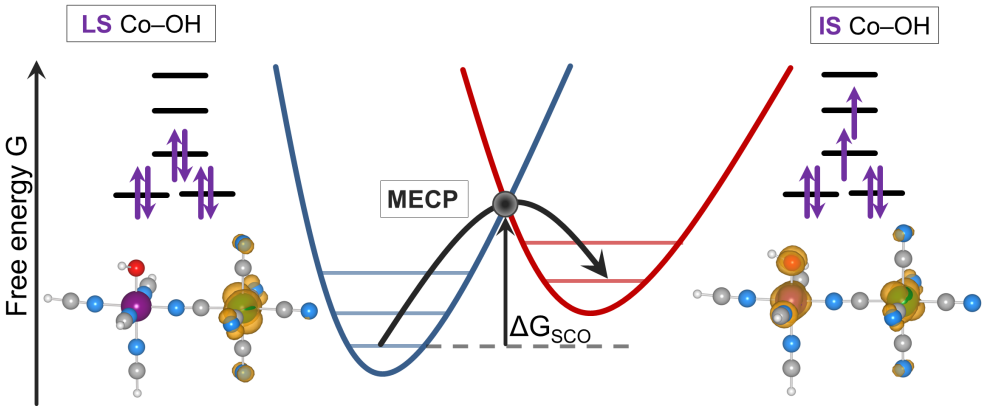


Figure 3: Spin-crossover (SCO) between LS *Co–OH and IS *Co–OH via the minimum energy crossing point (MECP), for which the SCO energy $\Delta G_{SCO}$ is required. The corresponding spin densities, i.e., the density of unpaired electrons, is shown as in yellow on both sites (isosurface = 0.005). While the active Co site in LS *Co–OH accomodates no excess unpaired electrons, IS *Co–OH clearly does, and therefore allows for more efficient electron transfer to form the subsequent *Co–O intermediates.

This opens up the possibility of a new OER pathway, an SCO-assisted pathway (Figure 4): Here, LS *Co–□ gets oxidised to LS *Co–OH ($OER\,1$), where it resides. Through SCO, LS *Co–OH transitions to IS *Co–OH, which then oxidises to LS *Co–O. This step ($OER\,2$) is still the most energetically demanding but now requires a much lower overpotential of $\eta = 0.26$ V. From there, the second water adsorption ($OER3$) and the $O_2$ desorption ($OER4$) proceed as usual. Although with a $\Delta G_{SCO}$ of around 0.45 eV the LS to IS transition of *Co–OH can happen at room temperature, the resulting IS state would immediately fall back to the LS state, as LS *Co–OH is much lower in energy than subsequent oxidation to *Co–O ($OER\,2$) as in Figure 4a. However, if the $OER\,2$ step becomes thermodynamically more favoured by applying an external potential, it will be more likely to happen. At potentials larger than the required onset potential ($U_{appl} > 1.23 + \eta$), the reaction goes downhill, and

once spontaneous thermal excitation to the IS state occurs, it becomes more likely to form the *Co–O intermediate from IS *CoFe–OH. This is shown in Figures 4b for $U_{appl}$ = 1.5 $V_{SHE}$. When LS *Co–OH transitions to IS *Co–OH, all subsequent steps are thermodynamically downhill and consequently happen spontaneously. In this mixed, SCO-assisted pathway, the entire OER is favourable at 1.5 $V_{SHE}$.

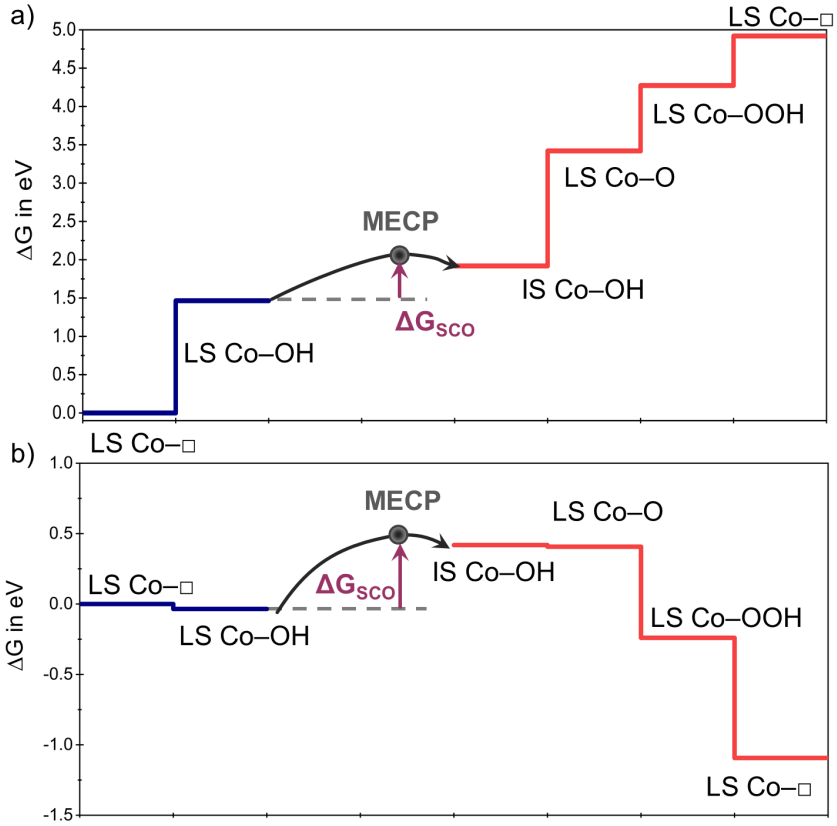


Figure 4: Standard free energy diagrams for the SCO-assisted OER at (a) zero applied potential U = 0 $V_{SHE}$ and (b) at U = 1.5 $V_{SHE}$, when we allow for a minimum energy crossing between LS *Co–OH and IS *Co–OH. If SCO from LS *Co–OH to *Co–OH has happened and the energy of the PDS is reduced when applying an external voltage of 1.5 $V_{SHE}$, all electrochemical reaction steps (not the SCO) are energetically downhill.

All in all, such SCO-assisted pathway can reduce the thermodynamic overpotential $\eta$ by nearly 0.5 V, resulting in an overpotential of only about 0.3 V, which is in agreement with experiments.[34,36,37] Indeed an electrocatalytic pathway involving SCO has recently been found for Fe centres in the ORR,[29] detected by different operando spectroscopies. Multiple rea-

sons that induce the SCO come into question, e.g., temperature, pressure, intercalated guest ions, and applied fields.[23–26] We hypothesize that the externally applied field contributes to the SCO,[33] which is aided by charge transfer transitions to and from Fe. The external potential stabilizes the higher spin-state IS *Co–OH because it has a higher capacitance than the LS *Co–OH.[51] This in turn is due to its higher electronic density of states close to the Fermi level, which results in a higher quantum capacitance as explained by Duan and Henkelmann.[28] Further, we propose a possible thermal enhancement, heating the sample would lead to an expansion of the Co–ligand bonds and thus weakening its crystal field, which would favour IS (and HS) states. Adding temperature would also facilitate to cross the activation barrier $\Delta G_{SCO}$ and allow for more catalytic centres to flip spin and attain the more active IS *Co–OH spin state. These possibilities remain to be tested and open up ample opportunities for further research on SCO-driven electrocatalysis.

# Conclusion

In summary, we show that a spin-crossover assisted OER pathway can significantly reduce the thermodynamic overpotential of cobalt hexacyanoferrate. Manipulating the spin configuration of the resting state gives us another handle for improving OER (and electrocatalysis in general) and allows us to overcome strict linear scaling relationships. Control over spin-crossover can be exerted experimentally through various factors, such as temperature, pressure, light, or an applied electric field. While spin-crossover has been widely investigated for information storage, it has only rarely been applied in electrocatalysis,[28,29,52] therefore leaving extensive space for future research. Compounds that can easily switch their spin polarization such as Prussian blue analogues are ideal candidates for magnetic tuning of electrocatalytic reactions. This, together with its stability and high OER efficiency, makes CoFe–PB an ideal and versatile water oxidation catalyst.

# Methods

The cobalt hexacyanoferrate (CoFe–PB) catalyst was represented by two different models, a solid surface slab (Figure 1a) and a bimetallic finite-size cluster (Figure 1b). Both were cut from a previously optimized bulk solid ($KCo[Fe(CN)_6]$), which is described in an earlier publication.[53] The periodic slab $Na_6Co(II)_6[Fe(III)(CN)_6]_6 \cdot 3\,H_2O$ contained three Co–Fe metallic layers, out of which the lowest two layers were fixed during geometry optimization, and a 15 Å vacuum region. The surface Co centres, except the active site, are coordinated by $H_2O$ to preserve their octahedral coordination, while all Fe centres always kept their full $-CN$ coordination sphere. The finite-size clusters represent the continuation of the solid. Its negatively charged $-NC^-$ ligands (on Co) were capped with hydrogen to form stable $-NCH$ ligands. During relaxation the outer N and C atoms were kept fixed. A more detailed description of the systems and justification for the choice of model systems is found in the SI. All structures have been uploaded to the ioChem-BD database under the DOI 10.19061/iochem-bd-1-229.[39]

Density Functional Theory (DFT) calculations were performed with the softwares VASP (Vienna Ab Initio Simulation Package, version 5.4.4)[54] for the solid surface and Gaussian 09[55] for the finite-size clusters. For the periodic slab we employed Projector Augmented Wave (PAW) pseudopotentials with small cores[56,57] and the PBEsol+U ($U_{Co}$ = 3 eV, $U_{Fe}$ = 5 eV) functional;[58] the Hubbard U parameters were previously optimized and fit to the bandgap.[59] The bimetallic clusters were calculated with the hybrid functional TPSSh,[60,61] which is a non-empirical meta-GGA functional with 10% of exact exchange. As basis sets we used def2TZVP for Co and Fe, and def2SVP for the other atoms.[62] Other parameters and convergence criteria are given in the SI.

# Acknowledgement

The authors thank the financial support of the Spanish Ministry of Science and Innova-

tion (RTI2018-101394-B-I00, the Severo Ochoa Centre of Excellence CEX2019-000925-S 10.13039/501100011033), and ... Projects JR? and further thank the Barcelona Supercomputing Centre (BSC-RES) for generous computational resources.

## Supporting Information Available

A listing of the contents of each file supplied as Supporting Information should be included. For instructions on what should be included in the Supporting Information as well as how to prepare this material for publications, refer to the journal's Instructions for Authors.

## References

(1) A Hydrogen Strategy for A Climate Neutral Europe. 2020; `https://ec.europa.eu/energy/sites/ener/files/hydrogenstrategy.pdf`.

(2) Man, I. C.; Su, H.-Y.; Calle-Vallejo, F.; Hansen, H. A.; Martinez, J. I.; Inoglu, N. G.; Kitchin, J.; Jaramillo, T. F.; Nørskov, J. K.; Rossmeisl, J. Universality in oxygen evolution electrocatalysis on oxide surfaces. *ChemCatChem* **2011**, *3*, 1159–1165.

(3) Li, J.; Ma, J.; Ma, Z.; Zhao, E.; Du, K.; Guo, J.; Ling, T. Spin Effect on Oxygen Electrocatalysis. *Adv. Energy and Sustainability Res.* **2021**, 2100034.

(4) McCrory, C. C. L.; Jung, S.; Peters, J. C.; Jaramillo, T. F. Benchmarking heterogeneous electrocatalysts for the oxygen evolution reaction. *J. Am. Chem. Soc.* **2013**, *135*, 16977–16987.

(5) Seh, Z. W.; Kibsgaard, J.; Dickens, C. F.; Chorkendorff, I.; Nørskov, J. K.; Jaramillo, T. F. Combining theory and experiment in electrocatalysis: Insights into materials design. *Science* **2017**, *355*.

(6) Yu, M.; Budiyanto, E.; Tüysüz, H. Principle of Water Electrolysis and Recent Progress of Cobalt, Nickel, and Iron-based Oxides for Oxygen Evolution Reaction. *Angew. Chem. Int. Ed.* **2021**,

(7) Craig, M. J.; Coulter, G.; Dolan, E.; Soriano-López, J.; Mates-Torres, E.; Schmitt, W.; García-Melchor, M. Universal scaling relations for the rational design of molecular water oxidation catalysts with near-zero overpotential. *Nature Commun.* **2019**, *10*, 1–9.

(8) Pérez-Ramírez, J.; López, N. Strategies to break linear scaling relationships. *Nat. Catal.* **2019**, 1–6.

(9) Gatard, V.; Deseure, J.; Chatenet, M. Use of magnetic fields in electrochemistry: a selected review. *Curr. Opin. Electrochem.* **2020**, *23*, 96–105.

(10) Zhang, Y.; Liang, C.; Wu, J.; Liu, H.; Zhang, B.; Jiang, Z.; Li, S.; Xu, P. Recent Advances in Magnetic Field-Enhanced Electrocatalysis. *ACS Appl. Energy Mater.* **2020**, *3*, 10303–10316.

(11) Wu, T.; Xu, Z. J. Oxygen evolution in spin-sensitive pathways. *Curr. Opin. Electrochem.* **2021**, *30*, 100804.

(12) Garcés-Pineda, F. A.; Blasco-Ahicart, M.; Nieto-Castro, D.; López, N.; Galán-Mascarós, J. R. Direct magnetic enhancement of electrocatalytic water oxidation in alkaline media. *Nat. Energy* **2019**, *4*, 519–525.

(13) Yan, J.; Wang, Y.; Zhang, Y.; Xia, S.; Yu, J.; Ding, B. Direct magnetic reinforcement of electrocatalytic ORR/OER with electromagnetic induction of magnetic catalysts. *Adv. Mater.* **2021**, *33*, 2007525.

(14) Sun, Y.; Wang, J.; Liu, Q.; Xia, M.; Tang, Y.; Gao, F.; Hou, Y.; Tse, J.; Zhao, Y. Itinerant ferromagnetic half metallic cobalt–iron couples: promising bifunctional electrocatalysts for ORR and OER. *J. Mater. Chem. A* **2019**, *7*, 27175–27185.

(15) Chen, R. R.; Sun, Y.; Ong, S. J. H.; Xi, S.; Du, Y.; Liu, C.; Lev, O.; Xu, Z. J. Antiferromagnetic inverse spinel oxide LiCoVO4 with spin-polarized channels for water oxidation. *Adv. Mater.* **2020**, *32*, 1907976.

(16) Chen, R. R.; Chen, G.; Ren, X.; Ge, J.; Ong, S. J. H.; Xi, S.; Wang, X.; Xu, Z. J. $SmCo_5$ with a Reconstructed Oxyhydroxide Surface for Spin-Selective Water Oxidation at Elevated Temperature. *Angew. Chem. Int. Ed.* **2021**, *60*, 25884–25890.

(17) Ghosh, S.; Bloom, B. P.; Lu, Y.; Lamont, D.; Waldeck, D. H. Increasing the efficiency of water splitting through spin polarization using cobalt oxide thin film catalysts. *J. Phys. Chem. C* **2020**, *124*, 22610–22618.

(18) Mtangi, W.; Kiran, V.; Fontanesi, C.; Naaman, R. Role of the electron spin polarization in water splitting. *J. Phys. Chem. Lett.* **2015**, *6*, 4916–4922.

(19) Mtangi, W.; Tassinari, F.; Vankayala, K.; Vargas Jentzsch, A.; Adelizzi, B.; Palmans, A. R.; Fontanesi, C.; Meijer, E.; Naaman, R. Control of electronsâĂŹ spin eliminates hydrogen peroxide formation during water splitting. *J. Am. Chem. Soc.* **2017**, *139*, 2794–2798.

(20) Pan, L.; Ai, M.; Huang, C.; Yin, L.; Liu, X.; Zhang, R.; Wang, S.; Jiang, Z.; Zhang, X.; Zou, J.-J. et al. Manipulating spin polarization of titanium dioxide for efficient photocatalysis. *Nature Comm.* **2020**, *11*, 1–9.

(21) Suntivich, J.; May, K. J.; Gasteiger, H. A.; Goodenough, J. B.; Shao-Horn, Y. A perovskite oxide optimized for oxygen evolution catalysis from molecular orbital principles. *Science* **2011**, *334*, 1383–1385.

(22) Wei, C.; Feng, Z.; Scherer, G. G.; Barber, J.; Shao-Horn, Y.; Xu, Z. J. Cations in octahedral sites: a descriptor for oxygen electrocatalysis on transition-metal spinels. *Adv. Mater.* **2017**, *29*, 1606800.

(23) Cirera, J. Guest effect on spin-crossover frameworks. *Rev. Inorg. Chem.* **2014**, *34*, 199–216.

(24) Sato, O.; Iyoda, T.; Fujishima, A.; Hashimoto, K. Photoinduced magnetization of a cobalt-iron cyanide. *Science* **1996**, *272*, 704–705.

(25) Aguilà, D.; Prado, Y.; Koumousi, E. S.; Mathonière, C.; Clérac, R. Switchable Fe/Co Prussian blue networks and molecular analogues. *Chem. Soc. Rev.* **2016**, *45*, 203–224.

(26) Boström, H. L. B.; Cairns, A. B.; Liu, L.; Lazor, P.; Collings, I. E. Spin crossover in the Prussian blue analogue $FePt(CN)_6$ induced by pressure or X-ray irradiation. *Dalton Trans.* **2020**, *49*, 12940–12944.

(27) Milocco, F.; De Vries, F.; Bartels, I. M.; Havenith, R. W.; Cirera, J.; Demeshko, S.; Meyer, F.; Otten, E. Electronic Control of Spin-Crossover Properties in Four-Coordinate Bis (formazanate) Iron (II) Complexes. *J. Am. Chem. Soc.* **2020**, *142*, 20170–20181.

(28) Duan, Z.; Henkelman, G. Surface Charge and Electrostatic Spin Crossover Effects in $CoN_4$ Electrocatalysts. *ACS Catal.* **2020**, *10*, 12148–12155.

(29) Li, X.; Cao, C.-S.; Hung, S.-F.; Lu, Y.-R.; Cai, W.; Rykov, A. I.; Miao, S.; Xi, S.; Yang, H.; Hu, Z. et al. Identification of the electronic and structural dynamics of catalytic centers in single-Fe-atom material. *Chem* **2020**, *6*, 3440–3454.

(30) Kawabata, S.; Nakabayashi, K.; Imoto, K.; Ohkoshi, S.-i. Spin crossover phenomenon in a three-dimensional cyanido-bridged $Fe^{I}I$–$Mo^{I}V$ assembly. *J. Appl. Phys.* **2021**, *129*, 105501.

(31) Shimamoto, N.; Ohkoshi, S.-i.; Sato, O.; Hashimoto, K. Control of charge-transfer-induced spin transition temperature on cobalt- iron Prussian blue analogues. *Inorg. Chem.* **2002**, *41*, 678–684.

(32) Cafun, J.-D.; Lejeune, J.; Baudelet, F.; Dumas, P.; Itié, J.-P.; Bleuzen, A. Room-Temperature Photoinduced Electron Transfer in a Prussian Blue Analogue under Hydrostatic Pressure. *Angew. Chem.* **2012**, *124*, 9280–9282.

(33) Sato, O.; Kawakami, T.; Kimura, M.; Hishiya, S.; Kubo, S.; Einaga, Y. Electric-field-induced conductance switching in FeCo Prussian blue analogues. *J. Am. Chem. Soc.* **2004**, *126*, 13176–13177.

(34) Pintado, S.; Goberna-Ferroán, S.; Escudero-Adán, E. C.; Galán-Mascarós, J. R. Fast and persistent electrocatalytic water oxidation by Co–Fe Prussian blue coordination polymers. *J. Am. Chem. Soc.* **2013**, *135*, 13270–13273.

(35) Galán-Mascarós, J. R. Water oxidation at electrodes modified with earth-abundant transition-metal catalysts. *ChemElectroChem* **2015**, *2*, 37–50.

(36) Han, L.; Tang, P.; Reyes-Carmona, Á.; Rodríguez-García, B.; Torréns, M.; Morante, J. R.; Arbiol, J.; Galan-Mascaros, J. R. Enhanced activity and acid pH stability of Prussian blue-type oxygen evolution electrocatalysts processed by chemical etching. *J. Am. Chem. Soc.* **2016**, *138*, 16037–16045.

(37) Alsaç, E. P.; Ülker, E.; Nune, S. V. K.; Dede, Y.; Karadas, F. Tuning the electronic properties of prussian blue analogues for efficient water oxidation electrocatalysis: experimental and computational studies. *Chem. Eur. J.* **2018**, *24*, 4856–4863.

(38) Álvarez-Moreno, M.; de Graaf, C.; Lopez, N.; Maseras, F.; Poblet, J. M.; Bo, C. Managing the computational chemistry big data problem: the ioChem-BD platform. *J. Chem. Inf. Model.* **2015**, *55*, 95–103.

(39) Hegner, F. S. Dataset: Spin crossover assisted water oxidation with CoFe–PB. 2022; https://doi.org/10.19061/iochem-bd-1-229.

(40) Cotton, F. A.; Wilkinson, G.; Murillo, C. A.; Bochmann, M. *Advanced Inorganic Chemistry*, 6th ed.; John Wiley & Sons, 1995.

(41) Nørskov, J. K.; Rossmeisl, J.; Logadottir, A.; Lindqvist, L. R. K. J.; Kitchin, J. R.; Bligaard, T.; Jonsson, H. Origin of the overpotential for oxygen reduction at a fuel-cell cathode. *J. Phys. Chem. B* **2004**, *108*, 17886–17892.

(42) Schilling, Mauro and Patzke, Greta R and Hutter, Jürg and Luber, Sandra, Computational Investigation and Design of Cobalt Aqua Complexes for Homogeneous Water Oxidation. *J. Phys. Chem. C* **2016**, *120*, 7966–7975.

(43) Steiner, U. E.; Ulrich, T. Magnetic field effects in chemical kinetics and related phenomena. *Chem. Rev.* **1989**, *89*, 51–147.

(44) Shuler, K. E. Adiabatic correlation rules for reactions involving polyatomic intermediate complexes and their application to the formation of OH ($2\Sigma+$) in the $H_2$–$O_2$ flame. *J. Chem. Phys.* **1953**, *21*, 624–632.

(45) Chrétien, S.; Metiu, H. $O_2$ evolution on a clean partially reduced rutile $TiO_2$ (110) surface and on the same surface precovered with $Au_1$ and Au2: The importance of spin conservation. *J. Chem. Phys.* **2008**, *129*, 074705.

(46) Sun, Y.; Ren, X.; Sun, S.; Liu, Z.; Xi, S.; Xu, Z. J. Engineering High-Spin State Cobalt Cations in Spinel Zinc Cobalt Oxide for Spin Channel Propagation and Active Site Enhancement in Water Oxidation. *Angew. Chem. Int. Ed.* **2021**,

(47) Sánchez-Grande, A.; Nguyën, H. C.; Lauwaet, K.; Rodríguez-Fernández, J.; Carrasco, E.; Cirera, B.; Sun, Z.; Urgel, J. I.; Miranda, R.; Lauritsen, J. V. et al. Electrically Tunable Reactivity of Substrate-Supported Cobalt Oxide Nanocrystals. *Small* **2022**, 2106407.

(48) Harvey, J. N.; Aschi, M.; Schwarz, H.; Koch, W. The singlet and triplet states of phenyl cation. A hybrid approach for locating minimum energy crossing points between non-interacting potential energy surfaces. *Theo. Chem. Acc.* **1998**, *99*, 95–99.

(49) Jaime Rodríguez-Guerra, J.; Funes, I. EasyMECP – Self-contained Python script for performing MECP (Minimum Energy Crossing Point) with Gaussian. 2020; https://github.com/jaimergp/easymecp.

(50) Hammond, G. S. A correlation of reaction rates. *J. Am. Chem. Soc.* **1955**, *77*, 334–338.

(51) Nong, H. N.; Falling, L. J.; Bergmann, A.; Klingenhof, M.; Tran, H. P.; Spöri, C.; Mom, R.; Timoshenko, J.; Zichittella, G.; Knop-Gericke, A. et al. Key role of chemistry versus bias in electrocatalytic oxygen evolution. *Nature* **2020**, *587*, 408–413.

(52) Appleby, A.; Savy, M.; Caro, P. The role of transition element multiple spin crossover in oxygen transport and electroreduction in porphyrin and phthalocyanine structures. *J. Electroanal. Chem.* **1980**, *111*, 91–96.

(53) Hegner, F. S.; Herraiz-Cardona, I.; Cardenas-Morcoso, D.; López, N.; Galán-Mascarós, J. R.; Gimenez, S. Cobalt hexacyanoferrate on $BiVO_4$ photoanodes for robust water splitting. *ACS Appl. Mater. Interf.* **2017**, *9*, 37671–37681.

(54) Hafner, J.; Kresse, G. *Properties of Complex Inorganic Solids*; Springer, 1997; pp 69–82.

(55) Frisch, M. J.; Trucks, G. W.; Schlegel, H. B.; Scuseria, G. E.; Robb, M. A.; Cheeseman, J. R.; Scalmani, G.; Barone, V.; Mennucci, B.; Petersson, G. A. et al. Gaussian 09 (Revision A. 02). *Gaussian Inc., Wallingford CT* **2016**,

(56) Blöchl, P. E. Projector augmented-wave method. *Phy. Rev. B* **1994**, *50*, 17953.

(57) Kresse, G.; Joubert, D. From ultrasoft pseudopotentials to the projector augmented-wave method. *Phy. Rev. B* **1999**, *59*, 1758.

(58) Perdew, J. P.; Ruzsinszky, A.; Csonka, G. I.; Vydrov, O. A.; Scuseria, G. E.; Constantin, L. A.; Zhou, X.; Burke, K. Restoring the density-gradient expansion for exchange in solids and surfaces. *Phys. Rev. Lett.* **2008**, *100*, 136406.

(59) Hegner, F. S.; Galán-Mascarós, J. R.; López, N. A database of the structural and electronic properties of Prussian blue, Prussian white, and Berlin green compounds through density functional theory. *Inorg. Chem.* **2016**, *55*, 12851–12862.

(60) Tao, J.; Perdew, J. P.; Staroverov, V. N.; Scuseria, G. E. Climbing the density functional ladder: Nonempirical meta–generalized gradient approximation designed for molecules and solids. *Phys. Rev. Lett.* **2003**, *91*, 146401.

(61) Staroverov, V. N.; Scuseria, G. E.; Tao, J.; Perdew, J. P. Comparative assessment of a new nonempirical density functional: Molecules and hydrogen-bonded complexes. *J. Chem. Phys.* **2003**, *119*, 12129–12137.

(62) Weigend, F.; Ahlrichs, R. Balanced basis sets of split valence, triple zeta valence and quadruple zeta valence quality for H to Rn: Design and assessment of accuracy. *Phys. Chem. Chem. Phys.* **2005**, *7*, 3297–3305.